Apparent topologically forbidden interchange of energy surfaces under slow variation of a Hamiltonian

Zhixin Lu,[*] Christopher Jarzynski,[†] and Edward Ott[‡]
University of Maryland, College Park, Maryland 20742, USA
(Received 20 October 2014; published 15 May 2015)

In this paper we consider the motion of point particles in a particular type of one-degree-of-freedom, slowly changing, temporally periodic Hamiltonian. Through most of the time cycle, the particles conserve their action, but when a separatrix is approached and crossed, the conservation of action breaks down, as shown in previous theoretical studies. These crossings have the effect that the numerical solution shows an apparent contradiction. Specifically we consider two initial constant energy phase space curves $H = E_A$ and $H = E_B$ at time $t = 0$, where H is the Hamiltonian and E_A and E_B are the two initial energies. The curve $H = E_A$ encircles the curve $H = E_B$. We then sprinkle many initial conditions (particles) on these curves and numerically follow their orbits from $t = 0$ forward in time by one cycle period. At the end of the cycle the vast majority of points initially on the curves $H = E_A$ and $H = E_B$ now appear to lie on two new constant energy curves $H = E'_A$ and $H = E'_B$, where the B' curve now encircles the A' curve (as opposed to the initial case where the A curve encircles the B curve). Due to the uniqueness of Hamilton dynamics, curves evolved under the dynamics cannot cross each other. Thus the apparent curves $H = E'_A$ and $H = E'_B$ must be only approximate representations of the true situation that respects the topological exclusion of curve crossing. In this paper we resolve this apparent paradox and study its consequences. For this purpose we introduce a "robust" numerical simulation technique for studying the complex time evolution of a phase space curve in a Hamiltonian system. We also consider how a very tiny amount of friction can have a major consequence, as well as what happens when a very large number of cycles is followed. We also discuss how this phenomenon might extend to chaotic motion in higher dimensional Hamiltonian systems.

DOI: 10.1103/PhysRevE.91.052913 PACS number(s): 05.45.−a, 45.05.+x, 45.20.Jj, 45.50.−j

I. INTRODUCTION

A. Background

The principle of adiabatic invariance is a key concept for Hamiltonian systems with one degree of freedom that depend slowly on time. According to this principle, under suitable circumstances, a system's energy will continually change so as to approximately maintain a constant action, $J = \oint p \cdot \mathrm{d}q$, in the current temporally frozen Hamiltonian. This approximation applies when the time scale for change in the Hamiltonian sufficiently exceeds the orbital period of the particle in the current frozen Hamiltonian.

Recently a particular protocol for the slow, cyclic variation of a Hamiltonian with one degree of freedom was proposed [1], which appears to have counterintuitive behavior. Reference [1] was originally motivated by earlier work on microcanonical "Szilard engines" [2] which exhibit the same counterintuitive behavior and which have been explored further in Ref. [3]. The proposed Hamiltonian was of the form

$$H(q,p;\vec{\lambda}) = \tfrac{1}{2}p^2 + V(q,\vec{\lambda}), \tag{1}$$

with the time variation of $\vec{\lambda}(t)$ slow, and the parameter vector $\vec{\lambda}$ returning to its initial value after one cycle, as specified in detail in Sec. I B. At the beginning of the cycle, imagine that a large number N_A of initial conditions are spread uniformly on the energy curve, $H(q,p;\vec{\lambda}(0)) = E_A$, and a second large number N_B are spread uniformly on another energy curve, $H(q,p;\vec{\lambda}(0)) = E_B$, where $E_A > E_B$, and therefore the curve $H = E_A$ encircles the curve $H = E_B$. Numerically, following the Hamiltonian dynamics of all these points through one cycle $\vec{\lambda}(0) = \vec{\lambda}(4\tau)$ (for later notational convenience we denote the cycle duration as 4τ), it is found [1] that at the end of the cycle, to a very good approximation, the vast majority of A points have the same final energy E'_A, which is smaller than the corresponding approximate energy E'_B of the vast majority of B points. Thus $E'_A < E'_B$ and the curve $H = E'_B$ encircles the curve $H = E'_A$ (see Fig. 1). Neglecting a very small fraction of points (which gets smaller as τ increases), it appears that the A and B points approximately lie on constant energy curves that have interchanged; that is, at $t = 0$ the curve of A points encloses the curve of B points, while at $t = 4\tau$ the curve of B points appears to enclose the curve of A points (see Fig. 1).

The situation described above shows that the action, which is adiabatically invariant under appropriate conditions, is changed through one cycle of the protocol ($J(E'_A) \neq J(E_A)$, $J(E'_B) \neq J(E_B)$). As discussed in Sec. I B and Refs. [4–15], the explanation for this change of action is that the cyclic protocol for $\vec{\lambda}(t)$ drives the system through separatrix-associated orbits with arbitrarily long time scales, thereby violating a necessary condition for action being adiabatically invariant.

The main significant feature that we wish to emphasize is that the A and B action curves appear to have interchanged. This point will be the focus of our paper. In particular, this result should be surprising because the uniqueness of

[*]zhixinlu@umd.edu
[†]cjarzyns@umd.edu
[‡]edott@umd.edu

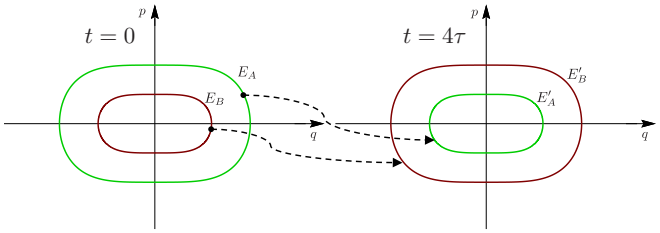

FIG. 1. (Color online) Apparent (not real) interchange of energy surfaces.

Hamiltonian orbits implies that orbits cannot cross one another in phase space. Thus a change such as that depicted in Fig. 1 is topologically forbidden. Hence, while Fig. 1 may apply in some approximate sense, the true situation must be different. Our question is: What is the nature of this difference and its dynamical origin?

B. Dynamics of the Hamiltonian

To realize the scenario described in Sec. I A, we consider a particle with one degree of freedom, described by the parameter-dependent Hamiltonian,

$$H(q,p;\vec{\lambda}) = \frac{p^2}{2} + V(q;\vec{\lambda}) = \frac{p^2}{2} + q^4 - \begin{cases} \lambda_L q^2 & \text{if } q \leqslant 0 \\ \lambda_R q^2 & \text{if } q \geqslant 0 \end{cases}, \tag{2}$$

where q is position, p is momentum, and $\vec{\lambda} = (\lambda_R, \lambda_L)$ are parameters that modulate the shape of the potential function $V(q;\vec{\lambda})$. As shown in Fig. 2, the time-dependent parameter vector $\vec{\lambda}(t)$ proceeds from (0,0) to (1,0) to (1,1) to (0,1) and back to (0,0), while the potential function deforms as shown in Fig. 3. More precisely, we take $\vec{\lambda}$ to vary with time as follows:

$$(\lambda_R,\lambda_L) = \begin{cases} \left(\frac{t}{\tau},0\right) & \text{if } 0 < t \leqslant \tau \quad \text{(phase 1)} \\ \left(1,\frac{t}{\tau}-1\right) & \text{if } \tau < t \leqslant 2\tau \quad \text{(phase 2)} \\ \left(3-\frac{t}{\tau},1\right) & \text{if } 2\tau < t \leqslant 3\tau \quad \text{(phase 3)} \\ \left(0,4-\frac{t}{\tau}\right) & \text{if } 3\tau < t \leqslant 4\tau \quad \text{(phase 4)} \end{cases}. \tag{3}$$

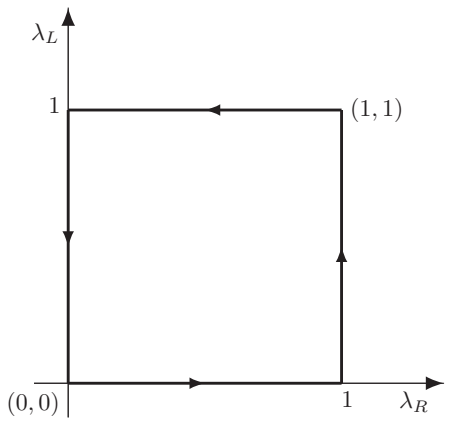

FIG. 2. The parameter vector $\vec{\lambda} = (\lambda_R,\lambda_L)$ starts from (0,0) when $t = 0$ and reaches (1,0) when $t = \tau$, (1,1) when $t = 2\tau$, (0,1) when $t = 3\tau$, and returns back to (0,0) when $t = 4\tau$. Each of the four phases of the full cycle has duration τ, and $\vec{\lambda}$ changes linearly with time during each of the four phases [Eq. (3)].

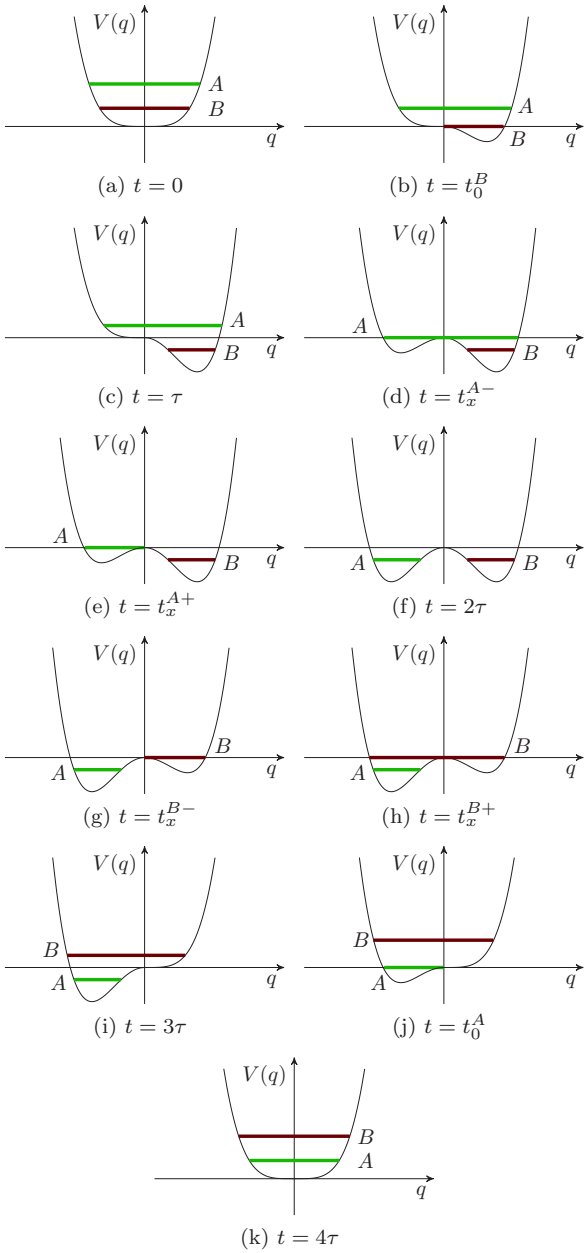

FIG. 3. (Color online) Snapshots at $t = 0$, t_0^B, τ, t_x^{A-}, t_x^{A+}, 2τ, t_x^{B-}, t_x^{B+}, 3τ, t_0^A, and 4τ. The green (light gray) and red (dark gray) horizontal lines represent set A and set B. Initially, set A is above set B, where the height represent the energy of the ensemble. At $t = 4\tau$, set B is above set A.

Since the Hamiltonian system is time dependent, the energy of the particle changes with time as

$$\frac{dE}{dt} = \frac{\partial H}{\partial q}\dot{q} + \frac{\partial H}{\partial p}\dot{p} + \frac{\partial H}{\partial \vec{\lambda}}\dot{\vec{\lambda}} = \frac{\partial H}{\partial \vec{\lambda}} \cdot \frac{d\vec{\lambda}}{dt}. \tag{4}$$

Thus, during phase 1 of the protocol ($0 < t \leqslant \tau$), the particle loses energy ($dE/dt = -q^2\tau^{-1}$) when it is traveling in the region $q \geqslant 0$, but it conserves its energy when $q < 0$. During phase 2 it loses energy when $q < 0$ and conserves energy when $q \geqslant 0$. During phase 3, the particle gains energy ($dE/dt = q^2\tau^{-1}$) when $q > 0$ and conserves energy when $q \leqslant 0$. During phase 4, it gains energy when $q < 0$ and conserves energy when $q \geqslant 0$. Upon completing the protocol, the energy of a particle is typically substantially changed from its initial value.

We choose two initial ($t = 0$) curves in (q,p) phase space: curve A and curve B defined as Hamiltonian level sets $H = E_A$, and $H = E_B$ [Figs. 3(a) and 4(a)], where, corresponding to these energies, the curves enclose areas in (q,p) phase space (actions) J_A and J_B that satisfy

$$0 < J_B < J_x < J_A < 2J_x. \tag{5}$$

Here J_x is the action enclosed by one lobe of the figure-8-shaped separatrix curve $H(q,p,\vec{\lambda} = (1,1)) = 0$, or $p^2/2 + q^4 - q^2 = 0$. Thus

$$J_x = 2\sqrt{2}\int_0^1 \sqrt{q^2 - q^4}\, dq = 2\sqrt{2}/3. \tag{6}$$

Considering a cycle of our protocol (Fig. 2), we now *define* a hypothetical adiabatic evolution for these phase space curves. This defined evolution is illustrated in Figs. 3 and 4. At all times curves A and B are curves of constant H. During phase 1 of our protocol [Figs. 3(a) to 3(c) and 4(a) to 4(c)], the energies corresponding to both curves decrease so as to conserve their enclosed actions (the adiabatic invariant). As shown in Figs. 3(b) and 4(b) there will be some time $t_0^B \in (0,\tau)$ when the energy of curve B changes sign, $E_B(t = t_0^B) = 0$. When $t = \tau$, under the condition given by Eq. (5), curve B is trapped in the $q > 0$ well of the potential function, while curve A is not [Figs. 3(c) and 4(c)].

During phase 2 of our protocol, the energy of curve B is constant, because the potential V remains fixed in the region $q \geqslant 0$. For $\tau < t < t_x^A < 2\tau$, the energy of curve A decreases to conserve its enclosed action. The time t_x^A (which corresponds to the pseudocrossing time defined in Ref. [8]) is defined as the time at which constancy of the action enclosed by curve A implies that the energy of curve A becomes $V(q = 0) = 0$, which corresponds to the dashed separatrix curve in Fig. 5. Motivated by the fact that particles lose energy when $q < 0$ (but not when $q > 0$) during phase 2, we define our hypothetical evolution to be such that curve A is located in $q < 0$ for $t_x^A < t < 2\tau$. This is illustrated in Figs. 4(e) and 4(f), and by the blue (dark gray) curve in Fig. 5. By this definition the energy of particles on curve A evolves continuously in time, but there is a discontinuity in the action enclosed by curve A, by the amount $J_x = 2\sqrt{2}/3$ as t crosses t_x^A [8]. Specifically, the action associated with curve A decreases discontinuously by the area of the right lobe of the $H(q,p;\vec{\lambda}(t_x^A)) = 0$ separatrix depicted as the gray-shaded area in Fig. 5 [see also Figs. 3(d), 3(e), 4(d), and 4(e) where t_x^{A-} and t_x^{A+} denote time instants just before and just after t_x^A]. For $t_x^A < t \leqslant 2\tau$, the enclosed action area of curve A is conserved. At the end of phase 2 ($t = 2\tau$), the two curves are trapped in different wells [Figs. 3(f) and 4(f)]. Curve B is trapped in the right well ($q > 0$) with action J_B, and curve A is trapped in the left well with action $J_A - J_x$.

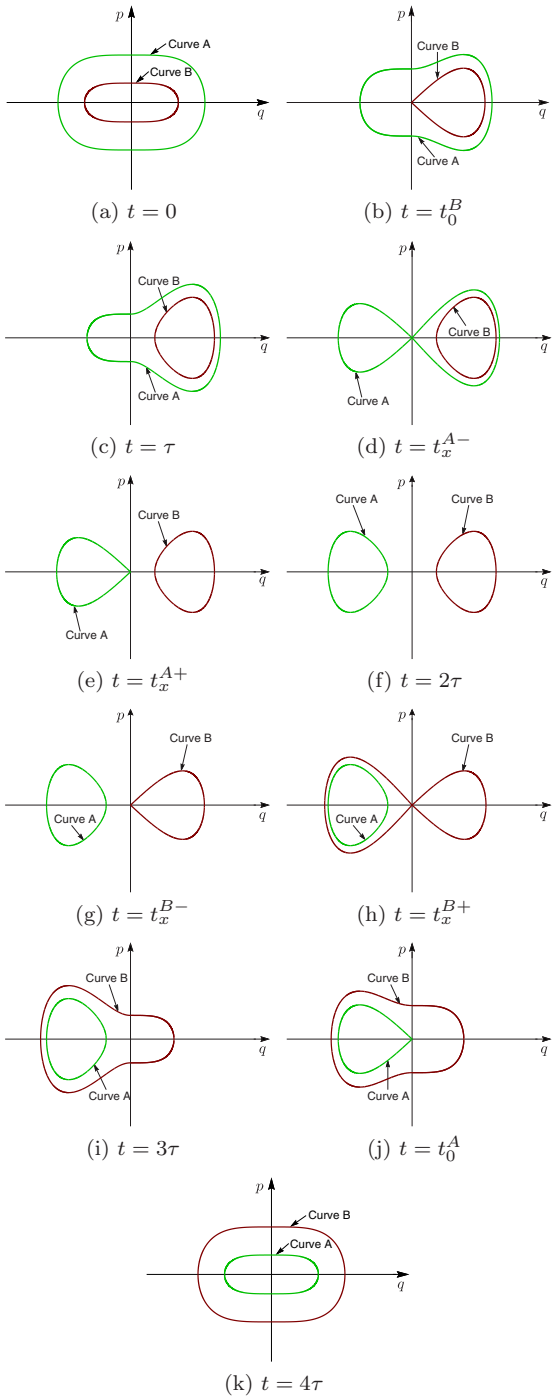

FIG. 4. (Color online) Assumed evolution of curve A and curve B when $t = 0$, t_0^B, τ, t_x^{A-}, t_x^{A+}, 2τ, t_x^{B-}, t_x^{B+}, 3τ, t_0^A, and 4τ.

During phase 3 of the protocol, for $2\tau < t < t_x^B$, the potential function increases on the $q > 0$ side and the energy of curve B increases maintaining constant action, becoming larger than the energy of curve A. Again, there is a time $t_x^B \in [2\tau, 3\tau]$ at which the energy of curve B reaches the value $V(q = 0) = 0$, and there is then a discontinuous increase in the action enclosed by curve B by the amount $J_x = 2\sqrt{2}/3$, similar to what is illustrated in Fig. 5 but with $q \to -q$ and the time ordering reversed; see Figs. 3(g), 3(h), 4(g), and 4(h). For

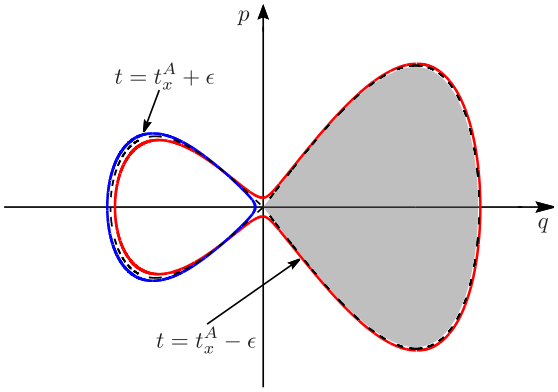

FIG. 5. (Color online) Discontinuity of the adiabatic action invariant of A particles at time t_x^A in the hypothetical evolution.

all subsequent time $t_x^B < t < 4\tau$ the enclosed actions of curves A and B remain constant [Figs. 3(i)–3(k) and 4(i)–4(k)], with values $J_A - J_x$ and $J_B + J_x$.

During phase 4, the left potential well rises, and the potential returns to its original quartic shape. We use $t_0^A \in (3\tau, 4\tau)$ to denote the time when the energy of curve A changes sign from negative to positive; see Figs. 3(j) and 4(j). Note that at $t = 4\tau$, the energy of curve B is higher than that of curve A [Figs. 3(k) and 4(k)]. Thus, proceeding through one cycle of the protocol, we have flipped the relative values of the energies and actions of the two curves. This flip is due to the two separatrix-crossing-induced action discontinuities: one at t_x^A decreasing the action of curve A, and the other at t_x^B increasing action for curve B. Specifically,

$$J_A(4\tau) = J_A(0) - J_x, \tag{7a}$$

$$J_B(4\tau) = J_B(0) + J_x, \tag{7b}$$

where $J_x = 2\sqrt{2}/3$ [see Eq. (6)] is the (q,p) area inside the right (left) separatrix lobe at $t = t_x^A$ ($t = t_x^B$). As shown by Eqs. (7), the initial A and B curves exactly interchange under the hypothetical evolution when $J_A(0) - J_B(0) = J_x$. While we could consider other values of $J_A(0) - J_B(0)$, for specificity, we have taken $J_A(0) - J_B(0) = J_x$ in Figs. 3–5.

As already noted (Sec. I A) and discussed in more detail in Sec. II, the hypothetical evolution illustrated in Figs. 3–5 cannot be entirely correct, as it violates the uniqueness and existence theorem of Hamiltonian dynamics. However, the analysis of Cary, Escande, and Tennyson [8] implies that this hypothetical evolution is, in a suitable sense, an approximation to the real dynamics. Specifically, in the limit of a very large number of initial conditions sprinkled on curves A and B, and a suitably large value of τ, if we remove from consideration a small fraction f of the particles, then the energies of the remaining particles never deviate from the energies resulting from our defined ideal evolution by more than some small quantity δ, and we can decrease f and δ with increasing cycle time so that $f \to 0$, $\delta \to 0$ as $\tau \to \infty$.

Indeed, the results of Ref. [8] imply that f decreases exponentially with τ.

These conclusions are supported by numerical evidence. We simulated 1000 Hamiltonian trajectories with initial conditions sampled from the energy surface $E_A = 0.2401$ and another 1000 trajectories with initial conditions sampled from $E_B = 0.0531$. Figure 6 shows the final conditions of these trajectories at the end of one cycle $t = 4\tau$ for different values of τ. At low τ [Fig. 6(a) for $\tau = 20$] the hypothetical curve evolution is seen to very poorly predict the result of the true dynamics. However, as τ is increased [Figs. 6(b)–6(d) for $\tau = 100, 500, 1000$] the hypothetical evolution provides an increasingly accurate description of the dynamics. Specifically, for Figs. 6(b)–6(d), there is a dense set of A particles colored in green (light gray) that seem to be tracing out a constant energy curve of energy E'_A that agrees well with the prediction of Eq. (7a), as well as a dense set of B particles colored in red (dark gray) that seem to be tracing out a constant energy curve of energy $E'_B > E'_A$, where the value of E'_B is predicted by Eq. (7b). Furthermore, in agreement with Ref. [8], we see that the E'_A and E'_B "curves" in Figs. 6(b)–6(d) have a width that decreases with increased τ implying that $\delta \to 0$ as $\tau \to \infty$. Using more sample points, we always see a small number of green (light gray) and red (dark gray) particles that are far from the constant energy E'_A and E'_B curves; we call such particles "delinquents." For instance, in Figs. 6(a)–6(b) some red (dark gray) points appear well within the interior of the region encircled by the $H = E'_B$ curve. In accord with Ref. [8], we see that the fraction of delinquents in Fig. 6 gets smaller with increasing τ (i.e., $f \to 0$ as $\tau \to \infty$).

C. Outline

The rest of this paper is organized as follows. Section II discusses the resolution of the topological issue raised above, that is, the interchange of the A and B curves, and evidence for the type of asymptotic validity ($f \to 0$, $\delta \to 0$ as $\tau \to \infty$) of the curve dynamics illustrated in Fig. 6. This is done partly by our introduction of a "robust" numerical simulation technique for studying the complex time evolution of a phase space curve in a Hamiltonian system. Section III notes that the adiabatic behavior for $\tau \gg 1$ is dramatically changed with a small amount of friction, and discusses the nature of this change. Section IV shows numerically the results of repeated cycling of this Hamiltonian system, which we relate to a theorem shown in Ref. [15]. Section V discusses how our work might be extended to chaotic motion in higher dimensional systems and summarizes our conclusions.

II. RESOLVING THE TOPOLOGY ISSUE

As discussed in Sec. I and illustrated in Fig. 6, for sufficiently large τ numerical simulations appear to be in agreement with the hypothetical evolution shown in Figs. 3 and 4, in which the curves A and B evolve through a sequence of action sets of the Hamiltonian. However, this defined dynamics cannot exactly correspond to the real dynamics in this slowly varying Hamiltonian since it violates two topological constraints. For example, see Ref. [8] for related discussion.

Most obviously, curve A encloses curve B at the beginning, yet curve A is enclosed by curve B at the end of the protocol. If this reflected the true dynamics, then every phase space orbit on the A curve would at some time have to cross an orbit on the B curve, which contradicts the uniqueness of solutions of Hamiltonians. [If there were an orbit crossing time, then

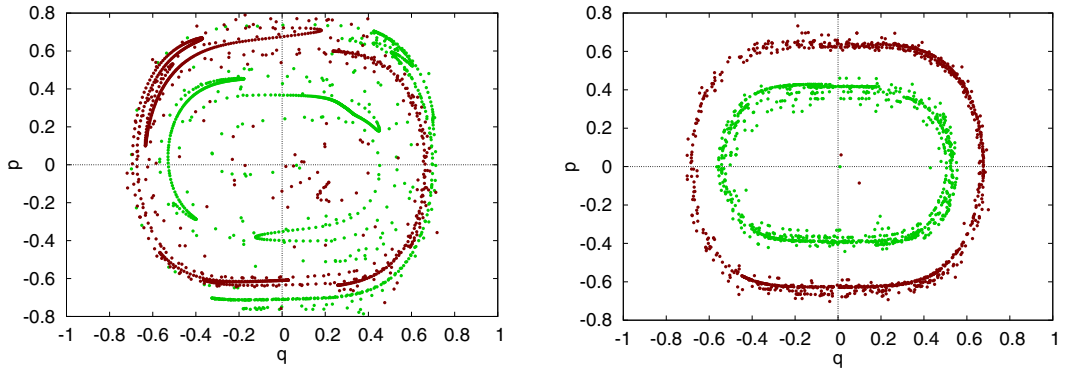

(a) $4\tau = 80$ (b) $4\tau = 400$

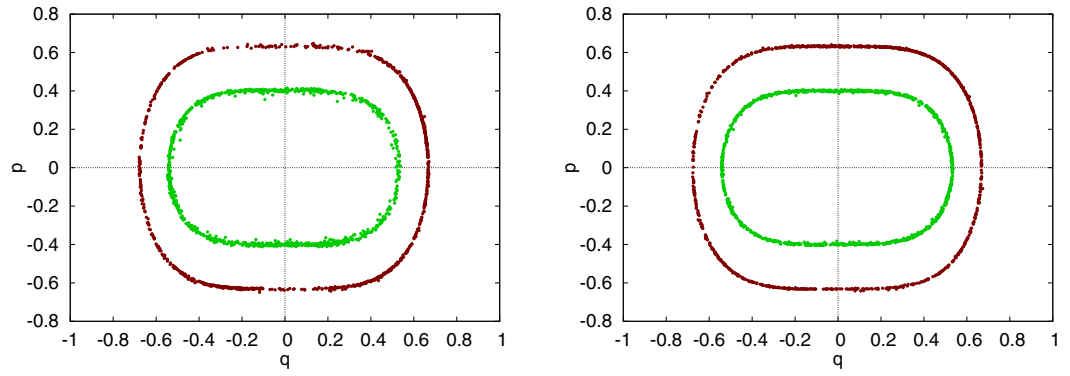

(c) $4\tau = 2000$ (d) $4\tau = 4000$

FIG. 6. (Color online) Final result at $t = 4\tau$ from regular simulation with different slowness parameters τ.

at this time an A particle and a B particle would have the same (q,p) value; then by evolving Hamiltonian's equations forward in time or backward in time from this crossing point, we would infer that the two orbits were identical for all time, thus contradicting the supposed existence of a crossing.] This violation of topology is visually evident in Fig. 4, as one proceeds from Figs. 4(c) to 4(i).

A less obvious topological violation occurs between $t = 0$ [Fig. 4(a)] and $t = \tau$ [Fig. 4(c)] and again between $t = 3\tau$ [Fig. 4(i)] and $t = 4\tau$ [Fig. 4(k)]. This violation arises because the origin $(q,p) = (0,0)$ is a fixed point; since $\partial V(q,t)/\partial q = 0$ at $q = 0$ for all time, a particle positioned exactly at $(p,q) = (0,0)$ at $t = 0$ would remain there throughout the cycle. Thus, under the true Hamiltonian dynamics, neither curve A nor curve B could pass through $(q,p) = (0,0)$, as they do several times during the hypothetical dynamics indicated in Figs. 4 and 5. The basic discrepancy between the hypothetical and the real evolution can be traced to the instants when curve A or B seemingly "crosses" the origin, as the condition of adiabaticity is then violated due to the fact that the orbit period in the frozen Hamiltonian approaches infinity.

In order to study the apparent "crossing" of $(q,p) \equiv (0,0)$, we consider the true dynamics when t approaches t_0^A or t_0^B. The part of the curve that is nearer to the origin moves slower than the part that is farther from the origin, since the origin is a fixed point of the dynamics. As a result, instead of crossing the origin, this curve is stretched and wound around the separatrix as it approaches the origin [see subsequent discussion of the blue (dark gray) curves in Figs. 7, 8, and inset to Fig. 8(f)]. The situation is somewhat similar when t approaches t_x^A or t_x^B, the difference being that the curve will be stretched and wound around, not the origin, but the separatrix lobe on the side where the potential function is stationary. In the simulations shown in Fig. 6, we uniformly put a finite number of sample particles on the initial curves and evolve them in the Hamiltonian system. The sample particles on the stretched portions of the curve eventually become sparse, and, if τ is too long, for any fixed numbers of points placed on the initial curves, some of them become too far separated to form a good approximation to the evolved "true" curve. Thus the true curves are eventually not resolved by these points, which are shown as red (light gray) dots in Figs. 7 and 8. This is why it appears that the evolved curves cross the origin and each other in the simulation. We will refer to a simulation employing a fixed number of sample points as a regular simulation.

In order to better reveal the true curve dynamics and show how a curve is wound around the origin or a separatrix lobe, we use a simulation method that we call "robust." In contrast to the regular simulation, the robust simulation monitors the distance between each pair of points that occur consecutively along the initial curve. When their separation d becomes larger than a critical value ε we add a new phase point halfway between them. The thin blue (dark gray) curves in Figs. 7 and 8 were obtained in this manner. Note that when part of the curve approaches the origin, it will experience greater curve stretching, and more phase points will be added to that part of the curve. Thus, in the robust simulations the curve made by joining consecutive phase points will always give a good

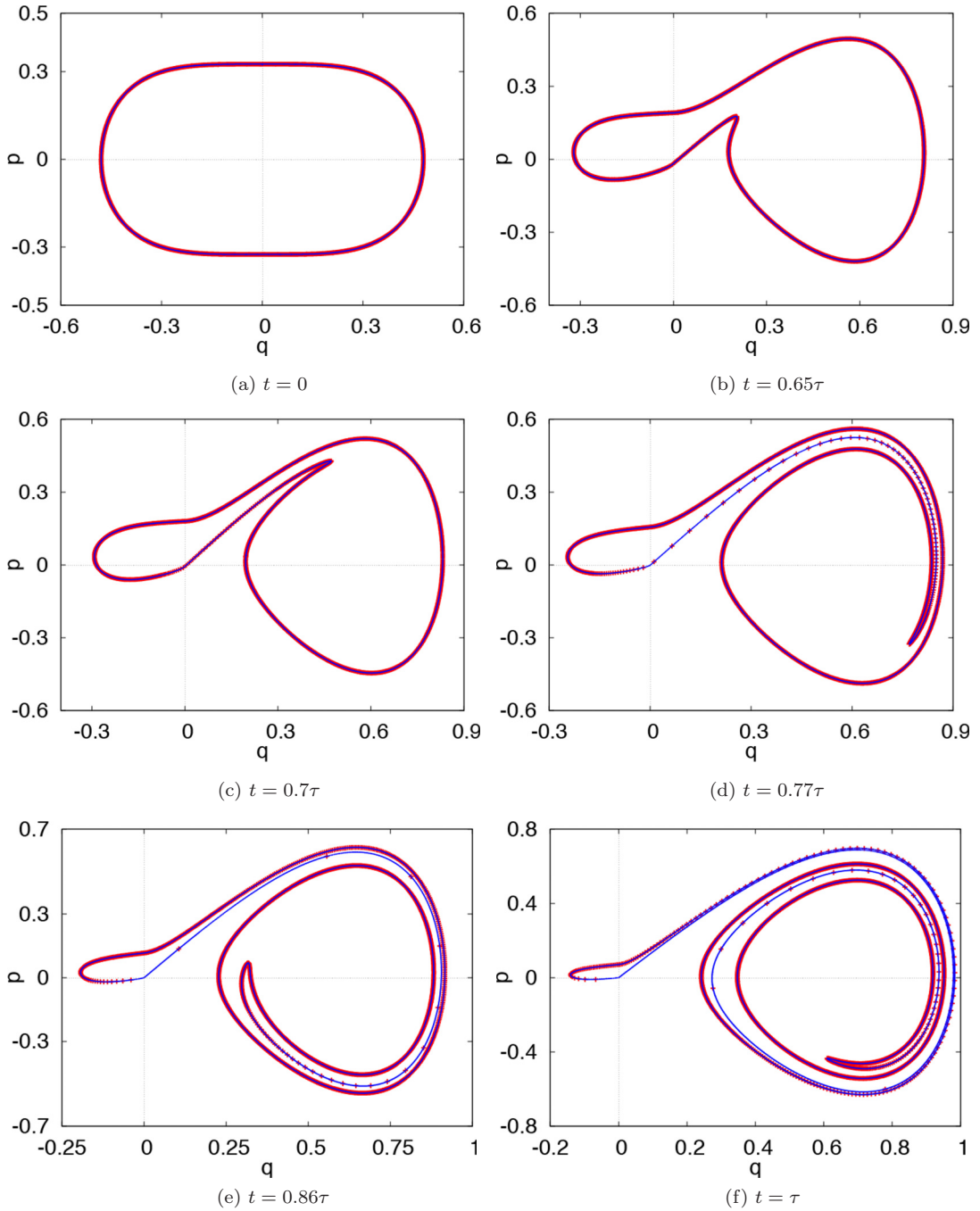

FIG. 7. (Color online) Six figures are snapshots in phase space showing the evolution of sample points along a positive energy curve at $t = 0$ to the resulting curve at $t = \tau = 20$, from both the regular and the robust simulations. The regular simulation evolves only those 2000 initial phase points. Its result is shown by the thick red (light gray) "curve," which is made up of 2000 red (light gray) points. The thin blue (dark gray) curve is the result from the robust simulation starting initially with 2000 points.

approximation to the true curve. The smaller the value of ε, the less sparse the curve. However, with too small ε, the simulation will require a large population of phase points. Thus, ε should be small enough that the curve is well resolved but allow reasonable computational cost. We also note that the number of phase points that are required by the robust simulations increases with increasing τ due to increase in the number of curve folds (compare Fig. 7 for $\tau = 20$ with Fig. 8 for $\tau = 200$).

During the first phase of the protocol, curve B approaches the origin when $t = t_0^B$. Figures 7 and 8 are snapshots of regular and robust evolution of energy curve B for $t \in [0,\tau]$ with $\tau = 20$ and $\tau = 200$, respectively. The red (light gray) dots from the regular simulation do not maintain a continuous curve, while the blue (dark gray) plots from the robust simulation do. It is clear that the true curve does not cross the origin, but is wound around it, as shown by the blue (dark gray) curve in Fig. 7 with $\tau = 20$ and the inset to Fig. 8(f). The same multifoil structure as in Fig. 7, but with more layers, appears in Fig. 8 where $\tau = 200$. We conclude that (i) the area enclosed by the true deformed curve is conserved (by Liouville's theorem),

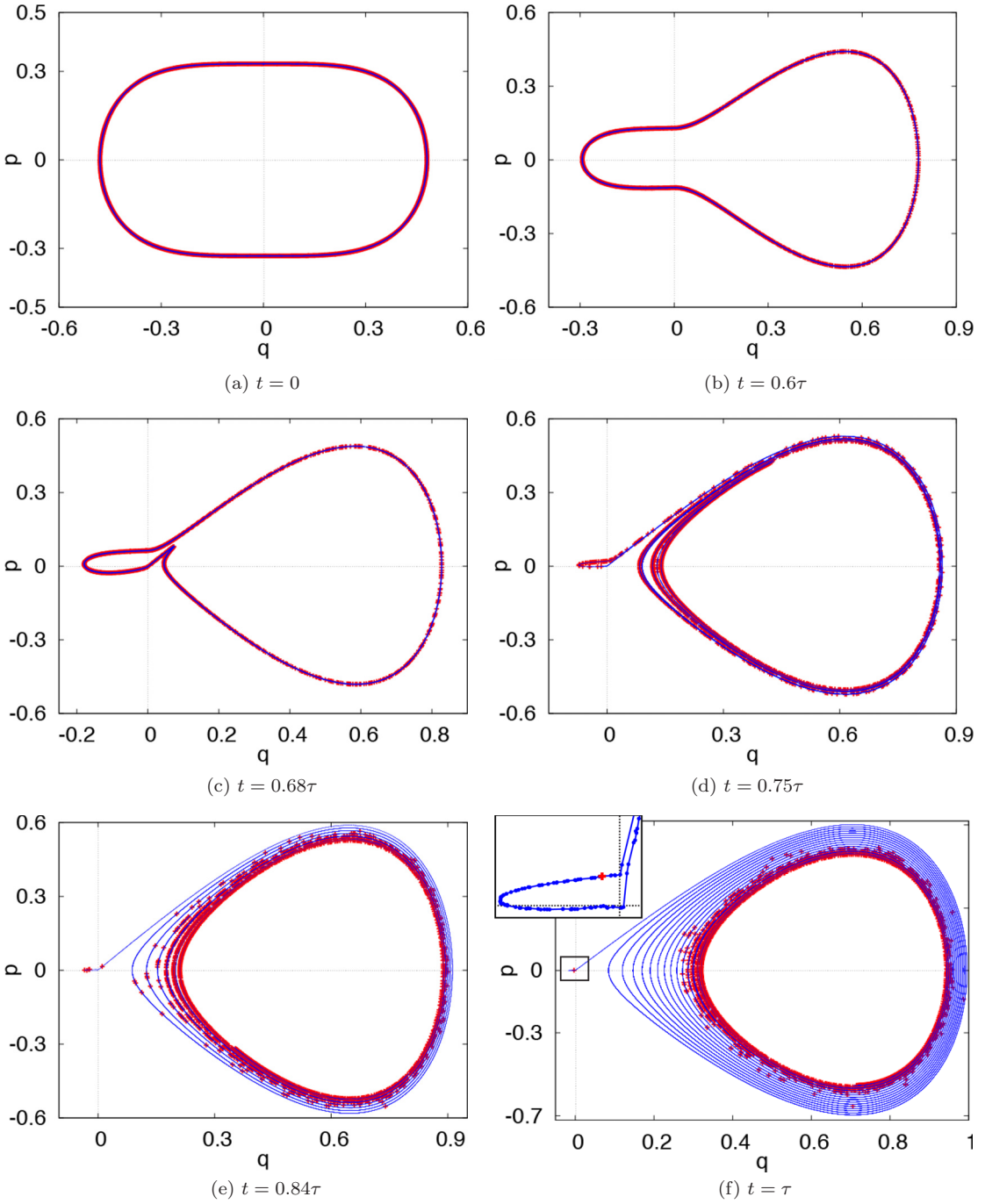

FIG. 8. (Color online) Snapshots for $0 < t < \tau$ with a larger $\tau = 200$. Red (light gray) points are results from regular simulation, and the blue (dark gray) thin curve is of robust simulation with $\epsilon = 0.0531$. The inset in panel (f) shows a magnification of the small rectangular near the origin, verifying that the origin $(q,p) = (0,0)$ is still enclosed by the true time-evolved curve at time $t = \tau$.

(ii) the multifoil structure has more layers with larger τ, and (iii) delinquents of the regular simulation are a small portion of phase points lying on the stretched foils [Fig. 8(f)]. For larger τ, the curve experiences greater stretching, while the proportion of delinquents becomes smaller, and most of the phase points stay near the curve predicted by the hypothetical evolution.

During the second phase ($t \in [\tau, 2\tau]$) in the hypothetical evolution, curve A "crosses" the separatrix orbit lobe on the $q > 0$ side together with the fixed point $(q,p) = (0,0)$ when $t = t_x^A$. This appears to happen in the regular simulation for the same reason we discussed for the first phase. A curve made of numerical sample particles from the regular simulation will appear to be broken when consecutive points move far apart as the true curve is stretched and wound around the separatrix lobe. To illustrate the real dynamics, we use the robust simulation for $t \in [\tau, 2\tau]$ and prepare an initial ($t = \tau$) curve A as specified in the hypothetical evolution [Fig. 4(c)]. In Fig. 9(a) the closed curve encloses area J_A that satisfies $J_x < J_A < 2J_x$. At the end of the second phase, the curve,

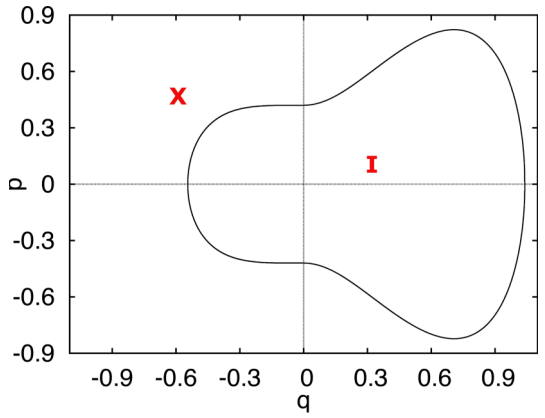

(a) $t = \tau$

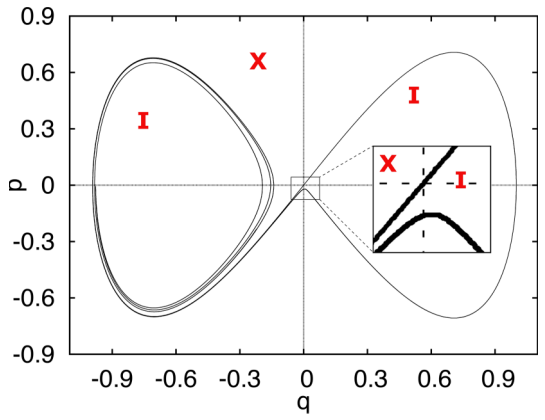

(b) $t = 2\tau$

FIG. 9. (Color online) Energy curve dynamics from a robust simulation illustrate the real dynamics of the separatrix "crossing" in the second phase. The insert shows a magnification about the origin for (b). The "X" and "I" symbols label regions that are exterior and interior to the closed curve; these designations are also used for Figs. 10–11.

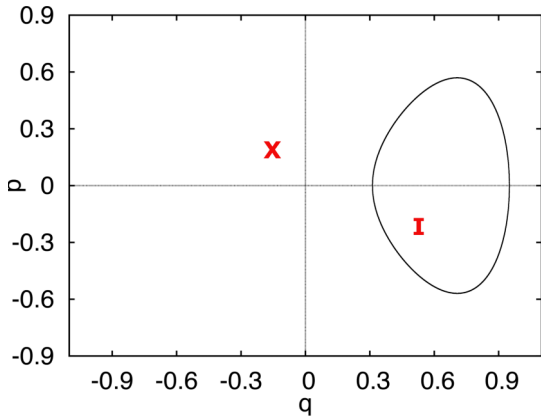

(a) $t = 2\tau$

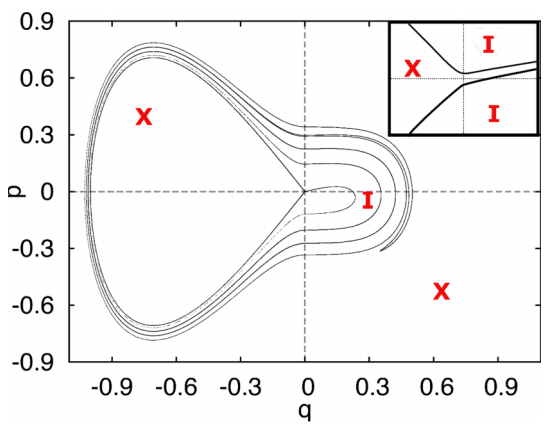

(b) $t = 3\tau$

FIG. 10. (Color online) Energy curve dynamics from robust simulation illustrates the real dynamics of the separatrix "crossing" in the third phase. A schematic illustration of a magnification around the origin is shown as the inset in panel (b).

as shown in Fig. 9(b), deforms into a curve enclosing both the right lobe of the separatrix orbit with an area J_x and a region on the left side. For $t_x^A < t \leqslant 2\tau$, the area on the left side that is enclosed by the true curve is well approximated by the area enclosed by the hypothetical curve. The fraction of particles in $q > 0$ from a regular simulation becomes very small for large τ, and the $q > 0$ lobe of area J_x eventually appears not to be encircled in a regular simulation. However, by Liouville's theorem the area enclosed by the deformed true curve is conserved. We obtain $J_A = J'_A + J_x$ where J'_A is the A action for the hypothetical evolution for $t > t_x^A$.

During the third phase in the hypothetical evolution [Figs. 4(f)–4(i)], curve B "swallows" the left separatrix orbit lobe and the separatrix point (origin) at time $t = t_x^B$ [Figs. 4(g)–4(h)]. During this phase of the evolution curve B gains energy, passing from negative to positive energies at $t = t_x^B$. To investigate the real dynamics, we initialized trajectories on the level surface $H = J_B(0)$ at time $t = 2\tau$, which corresponds to the red (dark gray) curve in Fig. 4(f). We then evolved this curve under the robust dynamics from $t = 2\tau$ to $t = 3\tau$. The results are shown in Fig. 10. The envelope of the curve in Fig. 10(b) has the same shape as the hypothetical red (dark gray) curve in Fig. 4(i). Most of the sample points from the regular simulation are near the envelope of the curve in Fig. 10(b), and there are a small number of delinquents, which we expect will disappear if τ is large enough. Although it is not obvious in the figure, the curve does not enclose the area confined by the left lobe of the separatrix orbit. Instead, it encloses the area confined within the multifoiled structure that has numerous layers.

During the fourth phase, curve A gains energy and seems to cross the origin in the regular simulation. This situation is similar that of curve B's "crossing" in the first phase, with the direction of the crossing being opposite. Curve A starts from inside the potential well on the right side and moves out at the end ($t = 4\tau$). Figure 11 shows how the curve in Fig. 11(a) at $t = 3\tau$ evolves by the end of the fourth phase, $t = 4\tau$. Notice that the curve becomes stretched and thus very thin. The curve that appears to terminate at the origin in Fig. 11(b) is not a single line but a folded curve enclosing the origin [see inset to Fig. 11(b)]. In the regular simulation, most of the particles lie close to the outer envelop of the structure shown in Fig. 11(b), while a small number of particles, the delinquents, can be found along the highly stretched foils.

Over the entire protocol, curves A and B experience the four deformations described above. Each deformation involves

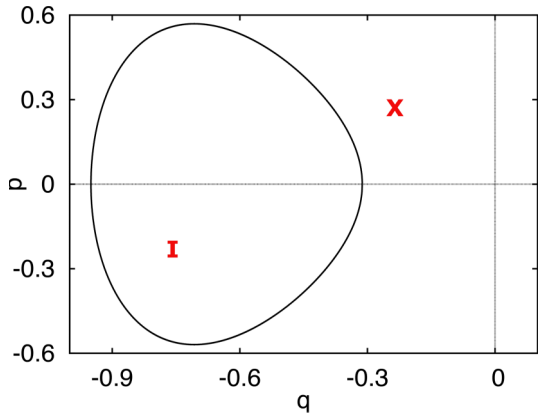

(a) $t = 3\tau$

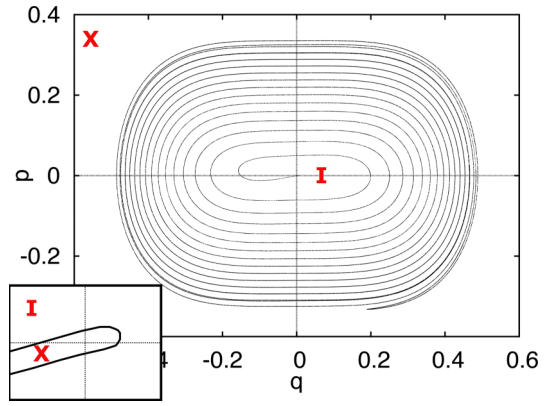

(b) $t = 4\tau$

FIG. 11. (Color online) Energy curve dynamics from robust simulation illustrates the real dynamics of the separatrix "crossing" in the fourth phase, starting with a Hamiltonian level curve of action $J_A(0) - J_x$ at time $t = 3\tau$. The inset shows a schematic illustration of a magnification around the origin of the robust curve calculation result at time $t = 4\tau$.

stretching a curve, A or B, as its energy approaches zero from above or below. The multifoil structures produced by these stretching deformations satisfy the topological constraints imposed by Hamilton's equations, while simultaneously explaining the apparent success of the hypothetical dynamics defined in Sec. I (Figs. 3 and 4). We have illustrated each deformation separately (Figs. 8–11), but when the system is subjected to the full protocol the four deformations occur in sequence, giving rise to a convoluted mixing of the curves A and B. When using robust simulations to study the evolution of both curves, we have found that for large τ (e.g., $\tau = 200$) the proliferation of phase points soon becomes excessive, and it is numerically infeasible to follow the full evolution through an entire cycle $[0,4\tau]$. However, for small enough τ we are able to simulate the cycle robustly. We show the results for $\tau = 20$ in Fig. 12. Although it is not evident to the eye, the evolving green (light gray) curve A encloses the red (dark gray) curve B at all times, and each curve remains topologically equivalent to a simple, closed loop enclosing the origin (0,0). A regular simulation is incapable of resolving the stretched, thin structure created by these dynamics.

III. MODEL WITH DAMPING

Although the regular dynamics approximately follows the hypothetical evolution when τ is large, adding a small amount of friction can change the evolution dramatically. In this case we consider the evolution,

$$\dot{q}(t) = p, \tag{8a}$$

$$\dot{p}(t) = -\frac{\partial H(q,p,t)}{\partial q} - \gamma p, \tag{8b}$$

where γ is the friction coefficient. Figure 13 show regular simulation results for $\tau = 1000$. Figure 13(a) has $\gamma = 0$, while Fig. 13(b) has $\gamma = 2 \times 10^{-5}$ (since $4\gamma\tau = 0.08$ the effect of friction over the cycle time is fairly small). As seen in Fig. 13(b), by adding friction, $\gamma = 2 \times 10^{-5}$, the result of a regular simulation is changed in an interesting way. Particles now appears to lie on four different energy curves instead of two. The two densest curves are close to the $\gamma = 0$ curves in Fig. 13(a), but there are additionally two sets of delinquents that appear to populate two other curves, with approximate actions J_x and $2J_x$. The impact of the friction term is negligible at all times except when t is close to t_x^A and t_x^B, when the seeming separatrix "crossings" occur. To understand this we will discuss the formation of the curve of green (light gray) delinquents that encircle the dense red (dark gray) curve in Fig. 13(b). [Similar considerations explains the presence of the curve of red (dark gray) delinquents occurring between the dense red (dark gray) and green (light gray) curves of Fig. 13(b).] To start, we notice that in Fig. 5 (for $t \simeq t_x^A$), when the A curve is about to cross the separatrix, it is very close to the right lobe of the separatrix, and its energy is slightly positive. As the trajectories corresponding to this curve gradually lose energy to friction, some of the trajectories in the region $q > 0$ acquire slightly negative energies, causing them to be trapped in the right well. Let us consider the fate of these delinquents during the remainder of the cycle. For $t_x^A < t < 2\tau$, these points remain in the right well, where the potential energy is not changing, and they evolve along approximately closed orbits enclosing an area J_x. At $t = 2\tau$ the potential in $q > 0$ begins to increase, and these trajectories now go over the potential hilltop at $q = 0$ and follow orbits that approximately encircle both the $q < 0$ and the $q > 0$ separatrix lobes. Thus for t slightly greater than 2τ these orbits now encircle an area corresponding to a total action of approximately $2J_x$. As t continues to increase, these orbits continually gain energy while at the same time conserving their action of approximately $2J_x$. At the end of the cycle, these trajectories are located along the curve of green (light gray) delinquents shown in Fig. 13(b). Similar considerations explain the "curve" of red (dark gray) delinquents. Thus adding friction not only increases the number of delinquents but also changes the distribution of sample particles in phase space.

IV. REPEATED CYCLING OF THE PROTOCOL GIVEN BY EQS. (2) AND (3)

A. Evolution of the action distribution function

As we have seen, after a single cycle of the protocol given by Eqs. (2) and (3), the predictions of the hypothetical dynamics

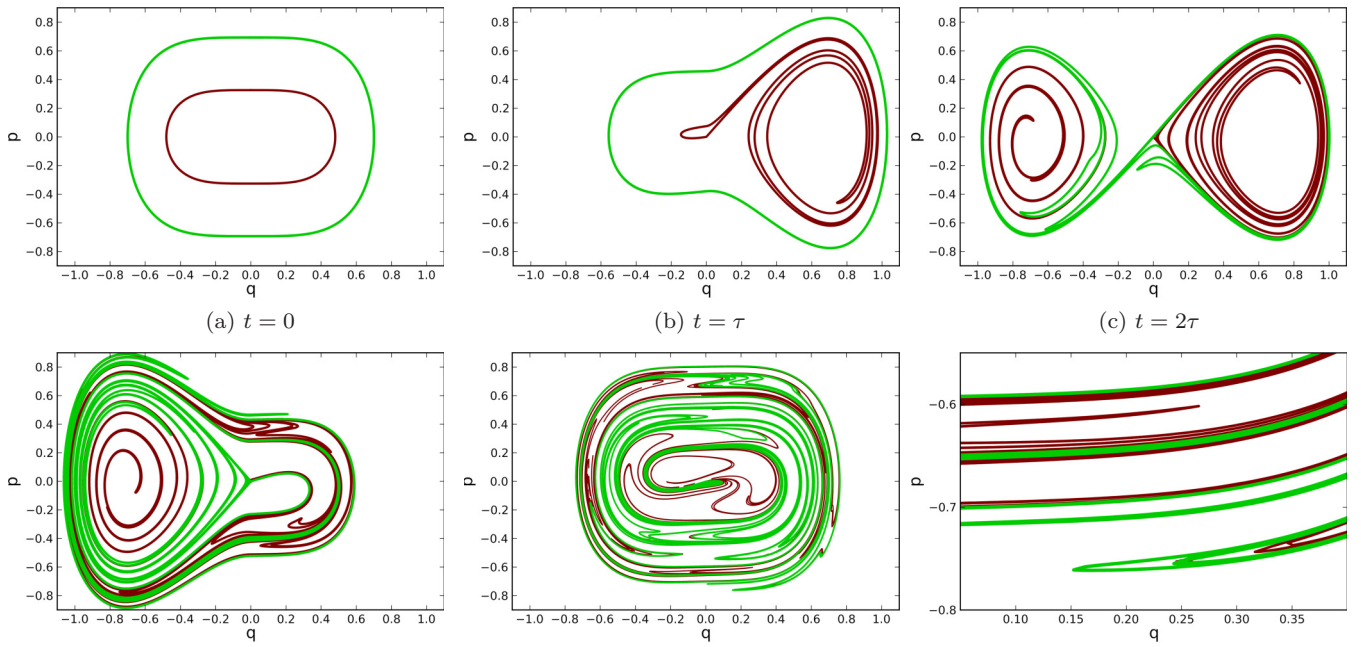

FIG. 12. (Color online) Snapshots for the full protocol with $\tau = 20$. Panel (f) is a zoom magnification of a small region of panel (e).

for curves A and B acquire some error. Although this error is small when τ is large, it can be expected to accumulate if the protocol is repeated over many cycles. The effect of repeated separatrix crossing on the distribution of action has also been studied in Refs. [14–17]. One of the important results is that in the limit of slow cycling, a Hamiltonian with a pulsating separatrix is chaotic in the region of phase space swept by the separatrix, and that the repeated separatrix crossings lead to diffusion of the adiabatic invariant [15]. To numerically investigate these anticipated effects in our system, we performed slow simulations ($4\tau = 2000$) in which trajectories were followed over 4000 cycles of the protocol. We used 20 000 trajectories, with initial conditions sampled from a curve enclosing $J_0 = 1.696$, and we monitored the evolution of the probability distribution of the action with time. Figure 14 shows this probability distribution of action after various numbers of cycles, from 50 to 4000. As shown in Fig. 14(a), after 50 cycles of repeated protocols, the width of the peak of the simulated action distribution originally located at the initial action value $J = J_0$ expands. From Figs. 14(a)–14(d), we also notice two other smaller peaks forming at $J = 0$ and $J = J_x$. This corresponds to the fact that each time a fixed point crossing (separatrix crossing) occurs, the "closed curve" formed by particles winds around the fixed point (separatrix lobe). Most of particles approximately follow the hypothetical dynamics so that they form a closed curve which seemingly crosses the fixed point (separatrix lobe), but a portion of particles remain close to the fixed point where $J = 0$ (the separatrix lobe where $J = J_x$) after this crossing. This is also seen in Fig. 8(f). After the fixed point crossing in the first phase, a red (light gray) particle still remains close to the fixed point. More generally [8], we expect that the number of particles that end up close to the fixed point

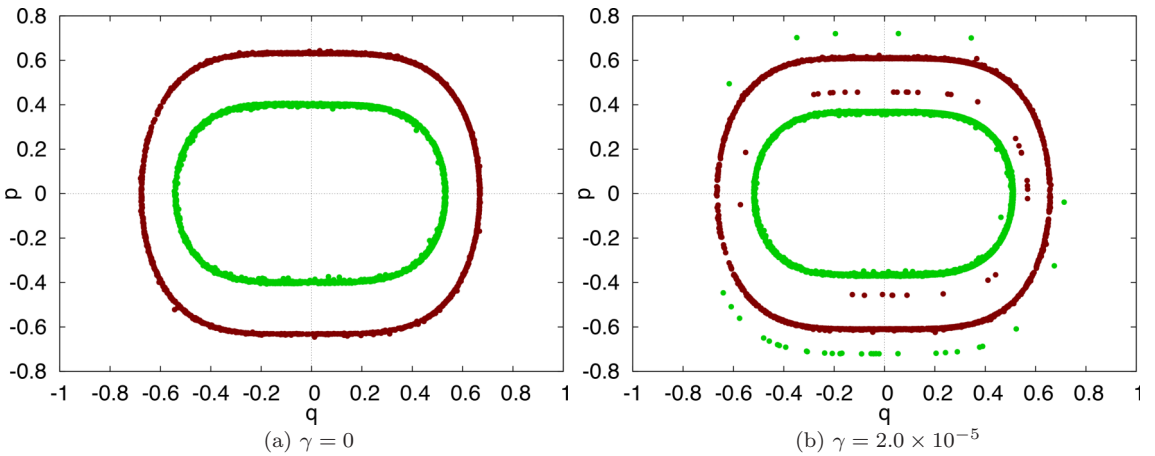

FIG. 13. (Color online) Result of two energy curves after going through the whole protocol with (b) and without (a) friction, $4\tau = 4000$ and $N = 2000$.

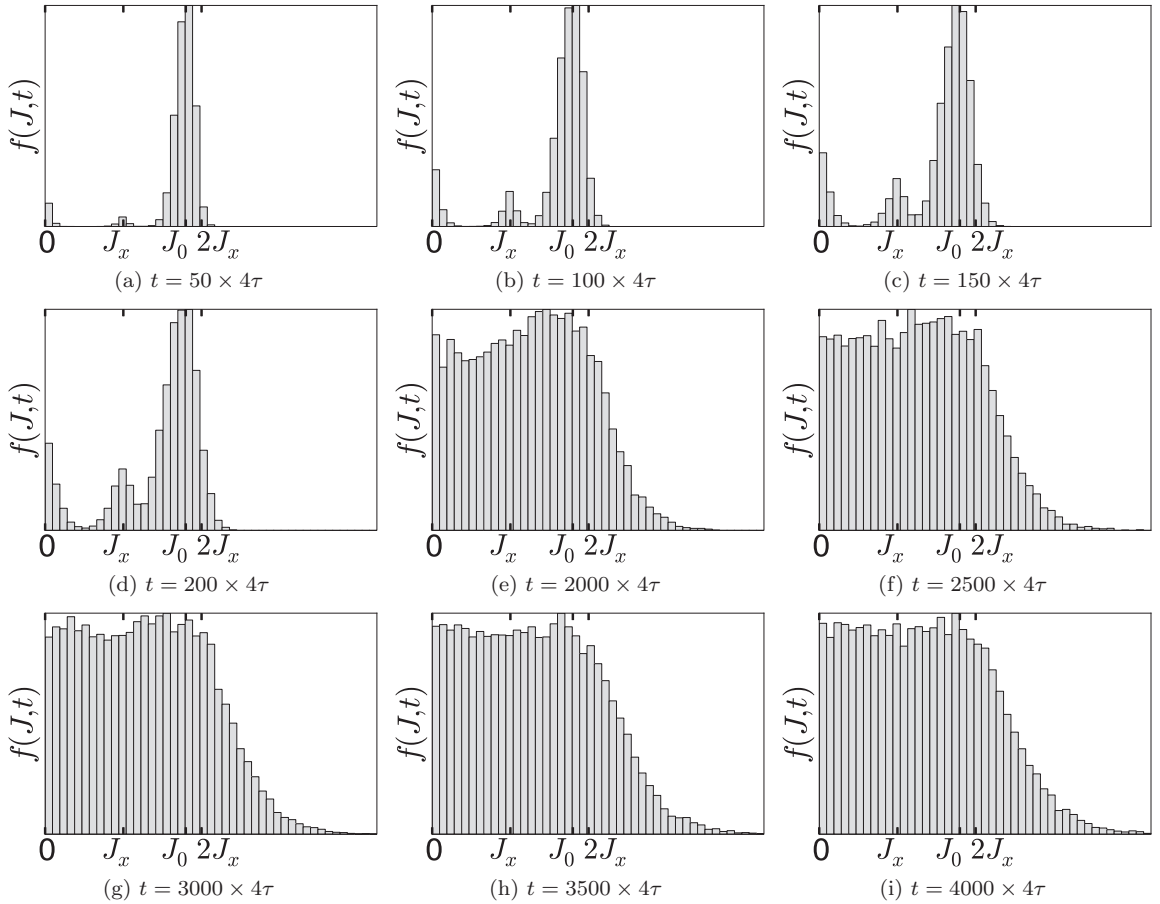

FIG. 14. Simulated histograms of action J after evolving the system different numbers of cycles.

or the separatrix lobe becomes smaller with larger τ. Since adiabaticity is spoiled by separatrix crossing and by the limited slowness of the simulation, the argument that a particle with initial action $J \in [0,2J_x]$ should continue to have its action in $[0,2J_x]$ is only true for most of particles, but not all. The simulated results show that with more and more cycles, an increasing number of particles end up with action exceeding $2J_x$. We see from Figs. 14(g), 14(h), and 14(i) that after 3000 cycles, the distribution becomes flat in $[0,2J_x]$ by the end of the simulation, while the tail in $J > 2J_x$ keeps growing.

The flat action distribution seen in Fig. 14 at large time for $J < 2J_x$ is consistent with the result of Refs. [8,15] that the dynamics is chaotic [15] and diffusive [8] in J in the phase space region swept by the slowly pulsating separatrix. Since the dynamics is sensitive to damping, we have used a fourth order symplectic integrator [18] to avoid the friction like numerical error from the regular RK4 integrator. A two-dimensional histogram in phase space at the end of 4000th cycle is shown in Fig. 15. Most particles are seen to be located within the energy curve enclosing area $J = 2J_x$.

B. Repeated cycling of the hypothetical curve dynamics with unequal well depths

We again consider the Hamiltonian, Eq. (2), but for the case where the left and right wells are of unequal depth. That is, the cycle through the square curve shown in Fig. 2, (λ_R,λ_L): $(0,0) \to (1,0) \to (1,1) \to (0,1) \to (0,0)$, is replaced by a rectangular-shaped cycle, (λ_R,λ_L): $(0,0) \to (\lambda_{R0},0) \to (\lambda_{R0},1) \to (0,1) \to (0,0)$, where $\lambda_{R0} \neq 1$. Thus, at the end of the second phase of the cycle (i.e., at $t = 2\tau$) the potential is as shown in Fig. 16.

Hence the separatrix lobes in Fig. 16 have different (q,p) areas: J_{xR} for the lobe in $q > 0$ and $J_{xL} > J_{xR}$ for the lobe in $q < 0$. We now consider the hypothetical curve dynamics obeyed by most points for τ large. Let J_n denotes the action

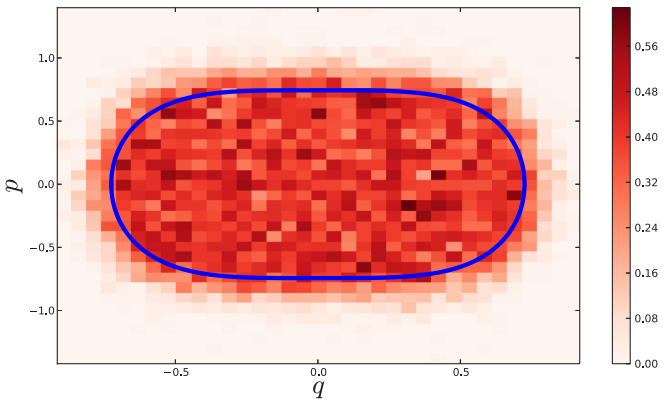

FIG. 15. (Color online) Simulated histogram in phase space after 4000 repeating cycles. The curve $J = 2J_x$ is shown in blue (dark gray).

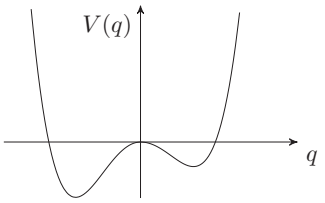

FIG. 16. The potential at $t = 2\tau$.

at the end of the nth cycle. Then for $0 < J_0 < J_{xL} + J_{xR}$ we have that $0 < J_n < J_{xL} + J_{xR}$ for all subsequent cycles. Furthermore, following the previous arguments in Sec. I B the hypothetical curve dynamics yields

$$J_{n+1} = \begin{cases} J_n + J_{xL} & \text{if } \ 0 \leqslant J_n < J_{xR} \\ J_n - J_{xR} & \text{if } \ J_{xR} < J_n < J_{xR} + J_{xL} \end{cases}. \quad (9)$$

Define $\theta_n = 2\pi J_n/(J_{xL} + J_{xR})$, $R = J_{xL}/(J_{xL} + J_{xR})$. Then Eq. (9) becomes

$$\theta_{n+1} = [\theta_n + 2\pi R] \ \textit{modulo}\ 2\pi. \quad (10)$$

Equation (10) can be viewed as describing successive rigid rotation of a circle by the angle $2\pi R$. If the rotation number R is rational, $R = m/l$, where m and $l < m$ are integers, then the orbit in θ is periodic with period l. For example, for the case $J_{xL} = J_{xR} \equiv J_x$ treated in Sec. IV A, $R = 1/2$, and J_n oscillates sequentially between two values separated by the amount J_x, with one value greater than J_x and one less than J_x. For R irrational, successive orbit points, θ_1, θ_2, θ_3, ..., generated by Eq. (10) ergodically fill the interval $0 < \theta < 2\pi$ densely and *uniformly* as $n \to \infty$. (In this case the orbit is said to be quasiperiodic [19].) Thus, starting from an initial condition $0 \leqslant J < J_{xL} + J_{xR}$, many cycles of the hypothetical curve evolution produce values of J that densely and uniformly fill the interval $0 < J < J_{xL} + J_{xR}$. Note that, as implied by the results in Sec. IV A, in order for the hypothetical curve dynamics (as described above) to be a good representation of the true dynamics, we require that τ be long and that n not be too large, with the limit on n increasing as τ becomes longer. In Fig. 17 we show numerical results of the histogram approximation of the action distribution function at times corresponding to different numbers of cycles, starting from an ensemble of 20 000 initial conditions uniformly distributed on the action curve $J_0 = 1.17$. We choose $\lambda_L = 1$ and $\lambda_R = (\sqrt{5} - 1)/2$ so that their ratio is an irrational number. As a consequence of the uniformity of the orbit density of J_n in $[0, J_L + J_R]$ for irrational R, we expect the action distribution function to approach uniformity fast in the interval $[0, J_L + J_R]$, as shown in Figs. 17(a)–17(e), with a slowly growing tail in $J > J_{tot}$, as shown in Figs. 17(e)–17(i).

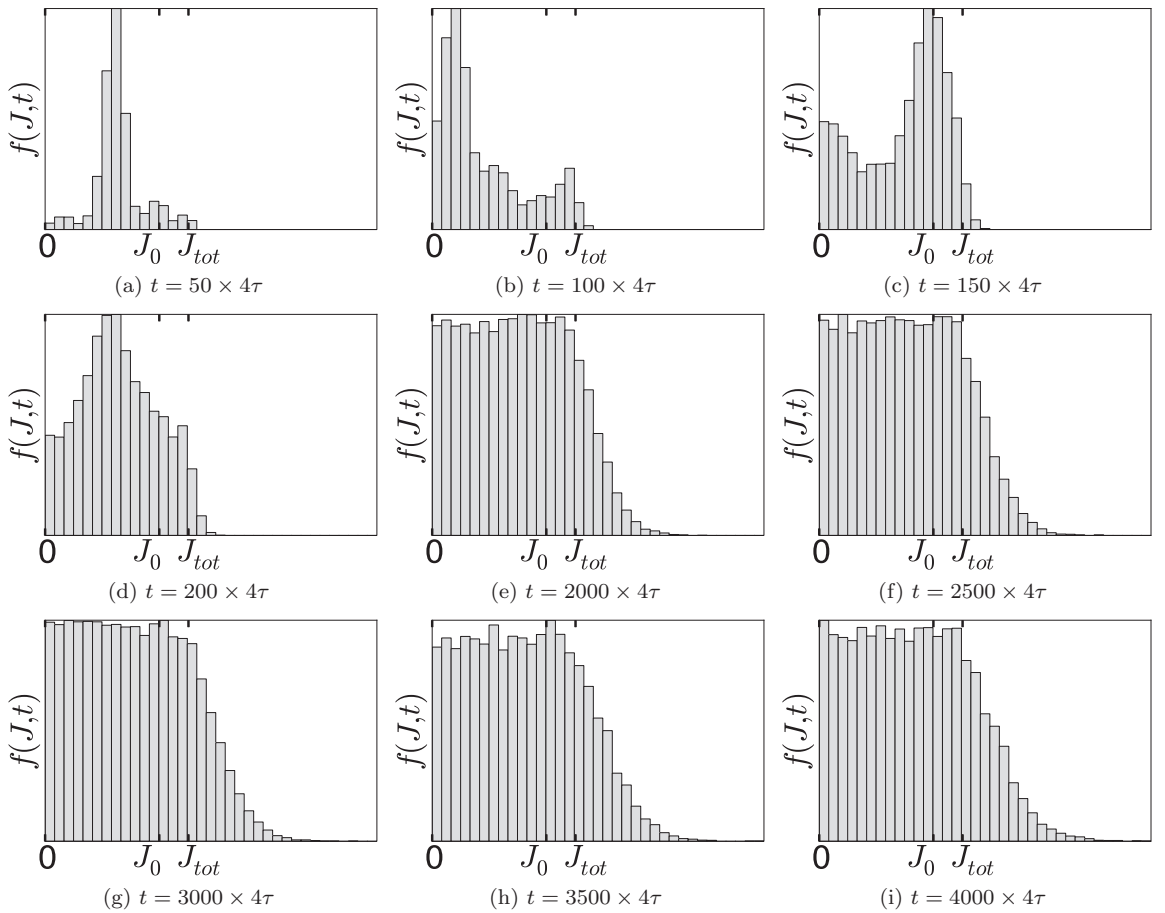

(a) $t = 50 \times 4\tau$ (b) $t = 100 \times 4\tau$ (c) $t = 150 \times 4\tau$

(d) $t = 200 \times 4\tau$ (e) $t = 2000 \times 4\tau$ (f) $t = 2500 \times 4\tau$

(g) $t = 3000 \times 4\tau$ (h) $t = 3500 \times 4\tau$ (i) $t = 4000 \times 4\tau$

FIG. 17. Simulated histograms of action J after evolving the system different numbers of cycles with unequal left and right well depths are shown. We use irrational ratio between well depths $(\lambda_L, \lambda_R) = (1, (\sqrt{5} - 1)/2)$. J_0 is the initial action value and $J_{tot} = J_L + J_R$.

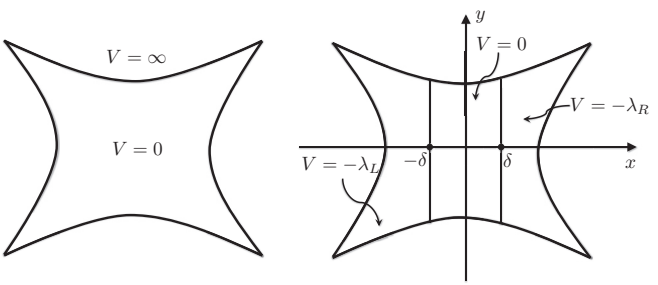

FIG. 18. Billiard system with unchanged potential and changing potential.

V. DISCUSSION OF A GENERALIZATION TO HIGHER DIMENSIONALITY AND CHAOTIC ORBITS

We can apply the general considerations of Sec. I to chaotic motion in higher dimensional systems by making use of the so-called Ergodic Adiabatic Invariant [20–22]. In this context, we consider Hamiltonian dynamics that is chaotic and ergodic over the energy surface. If the Hamiltonian evolves sufficiently slowly in time, at all times maintaining its chaotic and ergodic behavior, then the volume $\hat{J}$ of $(\vec{q},\vec{p})$ space enclosed by the energy surface is an adiabatic invariant. This applies as an approximation in the limit that the time it takes a chaotic orbit to wander over the energy surface in a reasonably dense manner is much shorter than the characteristic time over which the Hamiltonian changes.

As an example illustrating the Ergodic Adiabatic Invariant, consider a chaotic billiard in two spatial dimensions, as in Fig. 18(a) where there is a region of zero potential in the area enclosed by energy-conserving, specularly reflecting hard walls. Due to the concave shape of the walls, the orbit of a point mass M is typically chaotic and ergodic [e.g., randomly picking some time instant far past the time at which the particle orbit was launched, the spatial probability of the orbit location is typically uniform throughout the billiard area and the probability density of travel orientation is isotropic in $(0,2\pi)$]. The volume enclosed by the energy surface is

$$\hat{J} = 2\pi M E A_B, \tag{11}$$

where E is the particle energy and A_B is the spatial area of the billiard. If the walls of billiard change slowly with time so that $A_B = A_B(t)$, then the particle energy will change with time $E = E(t)$ so as to keep $\hat{J}$ approximately constant. (The error in this type of adiabatic invariant is considered in Refs. [20,21].)

To construct an example analogous to that of our one-dimensional problem, Eqs. (2) and (3) and Fig. 3, we consider the situation shown in Fig. 18(b) where there are three regions of spatially constant potential, $x > \delta$ with potential,

$$V_R = -\lambda_R(t), \tag{12}$$

$|x| < \delta$ with potential zero at all time, and $x < -\delta$ with potential,

$$V_L = -\lambda_L(t), \tag{13}$$

where $\vec{\lambda}(t) = (\lambda_R(t),\lambda_L(t))$ goes through the same cycle as Fig. 2 and Eq. (3). Thus at $t = 0$ the potential is zero everywhere; in the first phase $(0 < t < \tau)$ a well of negative potential and depth 1 forms in $x > \delta$; in phase 2 $(\tau < t < 2\tau)$ a similar well of depth 1 forms in $x < -\delta$; in phase 3 $(2\tau < t < 3\tau)$ the potential in $x > \delta$ is raised from -1 to zero thus removing the well in $x > \delta$; and in phase 4 $(3\tau < t < 4\tau)$ the potential in $x < -\delta$ is raised so as to return to the situation at the beginning of the cycle [see Fig. 19, which shows the potential versus x on the x axis $(y = 0)$]. Letting $\hat{J}_x = 2\pi M E A_x$ where A_x is the area of the left $(x < -\delta)$ or right $(x > \delta)$ well, and using the same reasoning as in the one-dimensional case (Sec. I B) we again obtain

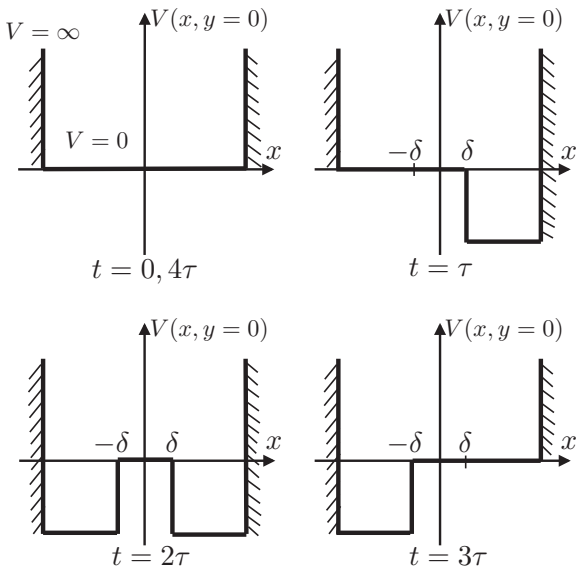

FIG. 19. Potential function for billiard system when $t = 0, \tau, 2\tau, 3\tau$, and 4τ.

$$\hat{J}_A(4\tau) = \hat{J}_A(0) - \hat{J}_x, \tag{14a}$$

$$\hat{J}_B(4\tau) = \hat{J}_B(0) + \hat{J}_x, \tag{14b}$$

for $2\hat{J}_x > \hat{J}_A(0) > \hat{J}_x > \hat{J}_B(0)$, which is the same as Eq. (7) with the (q,p) areas J replaced by the $(\vec{q},\vec{p})$ volumes $\hat{J}$. Thus this example displays the same type of topologically forbidden apparent interchange of energy surfaces as in the one-dimensional example (Sec. I).

It would be interesting to test this numerically. As opposed to the adiabatic motion associated with closed periodic orbits, the evolution in the case of ergodic adiabatic invariant has to be substantially slower (τ has to be longer) both because the chaotic ergodicity time to sample the whole energy surface can be long compared to a similar energy particle's period in a one-dimensional Hamiltonian, and because in the case of the one-dimensional adiabatic invariant the error can be exponentially small in τ, while for the ergodic adiabatic invariant the error scaling is much less favorable [20,21]. Thus numerical tests in this case might be challenging.

VI. DISCUSSION AND CONCLUSIONS

In this paper, in order to resolve the seeming paradox discussed in the Sec. I, we employ a simulation method we called "robust." The robust simulation evolves a large number of particles initially lying on an energy curve under the slowly

varying Hamiltonian. New particles are added if two originally neighboring particles become significantly separated during the evolution. With this simulation technique we demonstrate the following scenario, many of the main features of which we have related to previous theoretical work [4–17].

Before the fixed point (separatrix) crossing the curve of points very accurately approximates an energy curve with preserved enclosed phase-space area (action). However, upon the occurrence of the fixed point (separatrix) crossing, the curve deforms and winds around the fixed point (separatrix lobe). The part of the curve that winds around the fixed point (separatrix lobe) is greatly stretched and thus can hardly be seen in the regular simulation. This effect becomes stronger as the variation of Hamiltonian is made slower. Although a regular simulation accurately generates the dynamics of individual particle, it is unable to resolve the correct topological structure for the curve dynamics.

Some additional results are that (1) a small amount of friction can cause a large change in the dynamics; (2) consistent with Ref. [15], the effect of many repeated cycles of the protocol is to flatten the distribution of actions within the "adiabatically allowed" action range (Sec. IV A); (3) when the two wells have unequal depths, the ideal curve dynamics become quasiperiodic (Sec. IV); and (4) it appears possible that analogous phenomena may occur in higher dimensional system (Sec. V).

ACKNOWLEDGMENTS

C.J. acknowledges support from the National Science Foundation (USA) under Grant No. DMR-1206971. Z.L. is grateful to Zhiyue Lu and Shane Squires for useful and enjoyable discussions.

[1] S. Vaikuntanathan and C. Jarzynski, Phys. Rev. E **83**, 061120 (2011).
[2] R. Marathe and J. M. R. Parrondo, Phys. Rev. Lett. **104**, 245704 (2010).
[3] J. M. R. Parrondo and L. Granger, arXiv:1504.05388 [cond-mat.stat-mech].
[4] A. Neishtadt, Sov. Phys. Dokl. **20**, 189 (1975).
[5] A. Neishtadt, J. Appl. Math. Mech. **39**, 594 (1975).
[6] A. Neishtadt, Sov. J. Plasma Phys. **12**, 568 (1986).
[7] J. L. Tennyson, J. R. Cary, and D. F. Escande, Phys. Rev. Lett. **56**, 2117 (1986).
[8] J. R. Cary, D. F. Escande, and J. L. Tennyson, Phys. Rev. A **34**, 4256 (1986).
[9] J. Hannay, J. Phys. A: Math. Gen. **19**, L1067 (1986).
[10] A. N. Vasil'ev and M. A. Guzev, Theor. Math. Phys. **68**, 907 (1986).
[11] B. V. Chirikov, Proc. Roy. Soc. Lond. A **413**, 145 (1987).
[12] J. Henrard, in *Dynamics Reported* (Springer, Berlin, 1993), Vol. 2, pp. 117–235.
[13] B. Chirikov and V. Vecheslavov, J. Exp. Theor. Phys. **90**, 562 (2000).
[14] Y. Elskens and D. Escande, Physica D **62**, 66 (1993).
[15] Y. Elskens and D. F. Escande, Nonlinearity **4**, 615 (1991).
[16] C. R. Menyuk, Phys. Rev. A **31**, 3282 (1985).
[17] J. R. Cary and R. T. Skodje, Physica D **36**, 287 (1989).
[18] E. Forest and R. D. Ruth, Physica D **43**, 105 (1990).
[19] E. Ott, *Chaos in Dynamical Systems*, 2nd ed. (Cambridge University Press, Cambridge, 2002), Chap. 6.
[20] E. Ott, Phys. Rev. Lett. **42**, 1628 (1979).
[21] C. Jarzynski, Phys. Rev. Lett. **71**, 839 (1993).
[22] M. V. Berry and J. M. Robbins, Proc. Roy. Soc. Lond. A **442**, 659 (1993).